lated factors: (*a*) the reactivity of phenol toward the cyclic anhydride *versus* the reactivity of phenol toward the *in situ* formed acetic anhydride, and (*b*) the equilibrium concentration of acetic anhydride resulting from the solvolytic reaction of acetic acid with the cyclic anhydride. The more reactive the cyclic anhydride, the more readily it reacts with both phenol and acetic acid.

The present study provides a further quantitative picture of the effect of molecular structure on the partitioning between rate-determining formation and breakdown of the energy-rich tetrahedral intermediate for reaction at an acyl function. The poor leaving group tendency of the constrained neighboring carboxyl group in the reaction of phenol with cyclic anhydrides, due to the inclination of the neighboring carboxyl to undergo the reverse intramolecular reaction, resulted in tetrahedral intermediate breakdown being the rate-determining step. It is postulated that the good leaving group tendency of the unconstrained acetic acid in the reaction of phenol with the acyclic anhydride, acetic anhydride, results in tetrahedral intermediate formation being the rate-determining step. These differences in mechanism between the reactivity of cyclic and acyclic anhydrides in acetic acid compared to their hydrolytic reactivity must be due to the reduced ability of acetic acid, when compared to water, to solvate polar transition states.

## REFERENCES


(1) M. J. Haddadin, T. Higuchi, and V. Stella, *J. Pharm. Sci.*, **64**, 1759(1975).

(2) L. Eberson and L. Landström, *Acta Chem. Scand.*, **26**, 239(1972).

(3) E. Shami, J. Dudzinski, L. Lachman, and J. Tingstad, *J. Pharm. Sci.*, **62**, 1283(1973).

(4) A. E. Troup and H. Mitchner, *ibid.*, **53**, 375(1964).

(5) A. L. Jacobs, A. E. Dilatush, S. Weinstein, and J. J. Windheuser, *ibid.*, **55**, 893(1966).

(6) K. T. Koshy, A. E. Troup, R. N. Duvall, R. C. Conwell, and L. L. Shankle, *ibid.*, **56**, 1117(1967).

(7) J. Halmekoski and K. Vesalainen, *Farm. Aikak.*, **78**, 249(1969).

(8) J. Halmekoski and R. Mustonen, *ibid.*, **75**, 357(1966).

(9) "Dictionary of Organic Compounds," 4th ed., Oxford University Press, New York, N.Y., 1965.

(10) F. G. Baddar and L. S. Assal, *J. Chem. Soc.*, **1950**, 3606.

(11) S. Sunner and I. Wadsö, *Acta Chem. Scand.*, **13**, 97(1959).

(12) M. J. Haddadin, Ph.D. dissertation, University of Kansas, Lawrence, Kan., 1972, p. 8.

(13) R. Gandour, V. Stella, M. Coyne, and R. Schowen, Abstract 563 presented at the 10th Midwest Regional ACS Meeting, Iowa City, Iowa, 1974.

(14) T. C. Bruice and U. K. Pandit, *J. Amer. Chem. Soc.*, **82**, 5858(1960).

(15) M. L. Bender, U. L. Chow, and F. Chloupek, *ibid.*, **80**, 5380(1958).

(16) T. Higuchi, T. Miki, A. C. Shah, and A. Herd, *ibid.*, **85**, 3655(1963).

(17) T. Higuchi, L. Eberson, and J. McRae, *ibid.*, **89**, 3001(1967).

(18) T. C. Bruice and W. C. Bradbury, *ibid.*, **87**, 4838(1965).

(19) W. P. Jencks, "Catalysis in Chemistry and Enzymology," McGraw-Hill, New York, N.Y., 1969, pp. 8–15.

(20) T. C. Bruice and W. C. Bradbury, *J. Amer. Chem. Soc.*, **87**, 4846(1965).

(21) T. Higuchi, L. Eberson, and J. D. McRae, *ibid.*, **88**, 3805(1966).

(22) A. J. Kirby and P. W. Lancester, *J. Chem. Soc., Perkins Trans.*, **1972**, 1206.

(23) G. B. Barlin and D. D. Perrin, *Quart. Rev.*, **20**, 75(1966).


## ACKNOWLEDGMENTS AND ADDRESSES


Received January 8, 1974, from the *Department of Pharmaceutical Chemistry, University of Kansas, Lawrence, KS 66044*

Accepted for publication February 26, 1975.

Abstracted from a dissertation submitted by M. J. Haddadin to the University of Kansas in partial fulfillment of the Doctor of Philosophy degree requirements.

Supported in part by Alza Corp., Palo Alto, Calif.



* Present address: Department of Medical Sciences, University of Jordan, Amman, Jordan.

ˣ To whom inquiries should be directed


# Dissolution Patterns of Polydisperse Powders: Oxalic Acid Dihydrate


**J. T. CARSTENSEN ˣ and MAHENDRA PATEL**



**Abstract** □ The dissolution of oxalic acid dihydrate crystals of log-normal particle-size distribution in 0.1 *N* HCl was studied. A biphasic cube root dependence was found; the slopes of the initial cube root plots were consistent with theory based on dissolution of isometric, isotropic particles where assumptions were made of: (*a*) sink conditions, (*b*) particle-size-independent solubility, and (*c*) particle-size-independent film thickness of adsorbed liquid layers.



**Keyphrases** □ Dissolution of polydisperse powders (oxalic acid dihydrate)—dissolution patterns, equations □ Oxalic acid dihydrate (polydisperse powder)—dissolution patterns, equations □ Powders, polydisperse—dissolution, oxalic acid dihydrate, equations


The rates of dissolution and the mechanisms involved in the dissolution process have been the subjects of many publications in the last decade. However, most dissolution work done on powders has been restricted to monodisperse powders (1–4).

## BACKGROUND

Hixson and Crowell (5), basing their derivation on the Noyes–Whitney equation (6), arrived at the so-called cube root dissolution rate law:

$$\sqrt[3]{W_0} - \sqrt[3]{W} = Kt \qquad \text{(Eq. 1)}$$

where $W_0$ is the initial weight of the powder, $W$ is the weight of undissolved powder at time $t$, and $K$ is an apparent dissolution rate constant having units of $(\text{weight})^{1/3}$ per unit time. The assumptions made in the derivation of Eq. 1 are: (*a*) all particles dissolve isotropically, (*b*) the particles are isometric, (*c*) the thickness of the diffusion barrier around each particle (the "film thickness,"

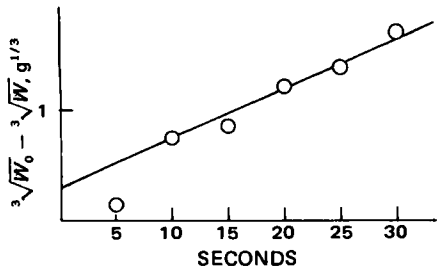


**Figure 1**—*Dissolution pattern of a "fine" powder of isothermally recrystallized oxalic acid dihydrate.*

$h$) is constant, ($d$) there are no particle-size solubility effects, and ($e$) sink conditions exist.

Most systems in pharmaceutical dosage forms are polydisperse systems; many investigators (7–12) have shown that particles prepared by procedures such as milling and precipitation produce skewed distribution functions which closely resemble log-normal particle-size distributions.

The dissolution of polydisperse powders of log-normal distribution was first studied by Higuchi and Hiestand (13) and Higuchi *et al.* (14). In their treatment, they approximated the log-normal frequency function:

$$f(\log x) = \frac{1}{\sqrt{2\pi}(\sigma)} \exp[(\log x - \log M)^2/2\sigma^2] \qquad \text{(Eq. 2)}$$

when expressed as a cumulative oversize distribution by the cumulative function:

$$g(x) = K/x^4 \qquad \text{(Eq. 3)}$$

where $x$ is the particle diameter, $M$ is the geometric mean diameter, and $\sigma$ is the standard deviation of the distribution. The nomenclature employed in Eq. 2 is adhered to in this study. Good agreement with experimental values was found previously using the approximation in Eq. 3 (13, 14).

Carstensen and Musa (15) generated log-normal distributions by computer and followed the dissolution under assumptions ($a$)–($e$); they found that the dissolution patterns could be approximated by a cube root law up to a critical time, $t_c$, when the smallest particle of diameter $a_0$ would be completely dissolved. Beyond this point, the cube root plot changes slope. The equation that held prior to the critical time was:

$$\sqrt[3]{W_0} - \sqrt[3]{W} = \frac{1.84kC_s \sqrt[3]{W_0}}{\sigma^{0.02}M\rho} t \qquad \text{(Eq. 4)}$$

where $C_s$ is the saturation concentration, and $k$ is the dissolution rate constant in centimeters per second. The distributions generated by Carstensen and Musa were all truncated (at + and $-3\sigma$). Equation 4 was found to hold in the limited range of $\sigma$ values tested; aside from the limitation of the $\sigma$ range tested, the equation[1] suffers from having the slope, $\alpha$, tend toward infinity when $\sigma$ tends toward zero.

Brooke (16, 17) arrived at an exact expression of the dissolution rate profile of a nontruncated, log-normal, particle-size distributed powder with the previously mentioned assumptions ($a$)–($e$). The treatment was expanded to truncated distributions by envoking the Hatch–Choate (11) equation; this equation is applicable when $\sigma < 0.14$ (18, 19). Brooke (17) also showed that a cube root relationship could be explained by the theoretically rigorous treatment and suggested the following equation:

$$\sqrt[3]{W_0} - \sqrt[3]{W} = \exp[-2.54\sigma_D^2] \frac{2kC_s \sqrt[3]{W_0}}{\rho M} t \qquad \text{(Eq. 5)}$$

where $\sigma_D = 2.3\sigma$. Brooke's equation has the same dependence on density, mean diameter, rate constant, initial weight, and solubility as that of Carstensen and Musa (15), but the dependence on standard deviation in Eq. 5 is different; it does not suffer from the limitations with which Eq. 4 is afflicted.

[1] The equation reported by Carstensen and Musa (15) contains an error in the exponent to $\sigma$ and in the numerical factor; the equation given here is correct in relation to the data reported in Ref. 15.

One main purpose of this study was to test whether real powders that do not contain spherical particles and do not (necessarily) adhere to assumptions ($a$)–($e$) follow a cube root law and, if so, whether Eqs. 4 and 5 are applicable to the dissolution profiles. Benet (20) pointed out that in spite of the theoretical work published to date, no experimental work other than that of Higuchi *et al.* (14) has been published.

The information obtained from dissolution of powders can be valuable regarding the bioavailability of oral dosage forms in solid or suspension form. Carstensen (4), using data from Prescott *et al.* (21), showed the relationship between the mean diameter of an orally administered powder and the fraction of drug absorbed.

## EXPERIMENTAL

The test substance used was oxalic acid dihydrate[2]. It was recrystallized by dissolving 100 g of oxalic acid in 200 ml of distilled water at 70° and cooling the solution at a rate of about 1°/10 min. This temperature was measured by a thermometer placed in the center of the beaker containing the solution. The temperature distribution by this procedure is very uneven (differing by as much as 15° between extreme points), giving rise to distributions that are somewhat off the log-normal distribution.

The suspension was allowed to stand for 24 hr at room temperature, and the crystals were then filtered off and air dried. The method produces crystals coarser than 70 mesh and as coarse as 4 mesh. The dried crystals were segregated into mesh fractions with USP sieves. To avoid vitrification[3], the fractions were stored in desiccators over saturated sodium chloride solution with excess sodium chloride (33% relative humidity). Oxalic acid dihydrate crystals of various mesh sizes were then blended in ratios that were log normal on a number basis.

The individual particle weights were obtained by weighing counted numbers of particles in each mesh fraction. A microscopic particle-size distribution was carried out on a random sample of particles from a −20/+30-mesh fraction. The density of oxalic acid was determined pycnometrically, using saturated oxalic acid solution as the liquid vehicle.

The general dissolution method was as follows. A 4-liter beaker was filled with 4 liters of 0.1 $N$ HCl and placed on a magnetic stirrer setup[4] equipped with a Teflon-coated stirring bar, 36 mm long and 8 mm in diameter; the solution was stirred at 400 rpm. This agitation condition allows the crystals to be suspended, whereas lower speeds do not accomplish good dispersion of the solid after it is added. The liquid in the beaker was equilibrated in a water bath at 25.8°[5] in a room at 25 ± 0.2°. Immediately prior to the start of the dissolution experiment, the beaker was transferred to the magnetic stirrer; 80 g of oxalic acid dihydrate powder was then added and the timing was started.

Approximately 6-ml samples were removed by hypodermic syringe at various time points. After removal, the sample was emptied into a test tube, exactly 5 ml was removed, and the oxalic acid content was determined by titration with 0.05 $N$ sodium hydroxide. In dissolution studies carried out at temperatures other than room temperature, the 0.1 $N$ HCl was measured out to 4 liters at room temperature and its temperature was then adjusted to the test temperature. Approximately 6-ml samples were taken as before, but 5 ml was not removed until the sample reached room temperature.

The solubility of oxalic acid dihydrate in 0.1 $N$ HCl was determined at various temperatures, and the determinations were made using a thermostated shaker bath[6].

The dissolution of a single crystal of oxalic acid was determined by placing it on a hemocytometer slide, adding 3 drops of 0.1 $N$ HCl, and observing the length, $L$, and breadth of the crystal microscopically as a function of time.

[2] Mallinckrodt analytical reagent oxalic acid dihydrate, Mallinckrodt Chemical Works, St. Louis, Mo.

[3] The water vapor pressure over the salt pair oxalic acid + oxalic acid dihydrate is 2.65 torr at 25° (22, 23), and the water vapor pressure over saturated oxalic acid solution is 23 torr (97% relative humidity) at 25° (24).

[4] Model 4812, solid-state magnetic 6 × 6 stirrer with thermostatically controlled hot plate, Cole Parmer, Chicago, IL 60648

[5] With the agitation conditions used, addition of 80 g of oxalic acid caused a temperature drop of 0.8°.

[6] Aquaterm water bath shaker model R-86, New Brunswick Scientific Co., New Brunswick, N.J.

Table I—Oxalic Acid Particles Used in a Particle-Size Distribution with Mean by Number of $M$ = 1500 μm and $SD$ = 0.108

| Mesh Fraction | Oversize Diameter, μm | Weight of Particles Used/80 g of Sample | Percent Particles by Number (Calculated) | Number of Particles/$10^8$ Particles |
|---|---|---|---|---|
| −5/+6 | 3360 | 1.33 | 0.065 | 54,000 |
| −6/+10 | 2000 | 31.13 | 12.44 | 12,439,000 |
| −10/+20 | 840 | 47.38 | 86.40 | 86,450,000 |
| −20/+30 | 590 | 0.16 | 1.09 | 1,057,000 |

## RESULTS AND DISCUSSION

It was mentioned previously (1) that substances, when crystallized from solution, tend to have particle sizes with a truncated log-normal distribution. Oxalic acid, when recrystallized isothermally from water, indeed shows a log-normal particle-size distribution. By varying the temperature at which the crystals are allowed to grow, it is possible to alter the mean particle size and standard deviation. However, the magnitudes of the standard deviations are all close so that if it were desired to study the effect of the standard deviation of a powder sample on its dissolution pattern, then isothermally recrystallized powders do not offer an approach that will allow a sufficiently wide variation in the variable to permit data analysis. Such powders, however, dissolve in a cube root fashion as predicted previously (15–17). The dissolution of a sample of isothermally recrystallized oxalic acid with a log-normal distribution, with a mean of 250 μm and a standard deviation of $\sigma$ = 0.13, is shown in Fig. 1.

It was predicted by computer simulation (15) that when $\sigma$ is not excessively large, a cube root plot of amounts undissolved *versus* time should give a biphasic linear plot. The point where the two lines intersect occurs at the critical time, $t_c$, corresponding to the point in time where the smallest particle of the original powder sample has just dissolved completely. It is noted in Fig. 1 that the cube root plot is quite linear but does not appear to be biphasic; on the other hand, it does not intercept at the origin but rather at a positive $y$ value. This result is due to the particles being too small (and the sample, in a relative sense, having too large a standard deviation) to allow detection of the initial phase.

Since attempts to grow particles of substantially larger mean diameters by isothermal recrystallization were not successful, larger crystals were grown nonisothermally. Log-normal populations were then obtained by sieving these coarser crystals and reblending the obtained fractions in ratios that were log normal on a number basis.

The data of numbers of particles from various mesh fractions used to produce these distributions are shown in Table I. The oxalic acid dihydrate crystals are not altogether regular in shape but appear microscopically to be parallelepipeds of length $L$ and breadth $B$ (Fig. 2).

A microscopic count from a −20/+30-mesh fraction is shown in Fig. 3. On the average, the length $L$ is 2.7 times the breadth $B$. The volume, $Q$, is $LB^2 = 2.7B^3$, and the dimension is $\sqrt[3]{Q} = (2.7B^3)^{1/3} = 1.39B$ (Table II). The dimensions correspond well with the mesh

Table II—Number Distribution of Crystal Volumes in a −20/+30 Fraction of Nonisothermally Crystallized Oxalic Acid Dihydrate Crystals

| Volume, (ml) × $10^{-3}$ | Dimension, $(Q/2.7)^{1/3}$, cm | Cumulative Percent | $SD$ |
|---|---|---|---|
| 0.3 | 0.048 | 10 | −1.28 |
| 0.5 | 0.057 | 20 | −0.84 |
| 0.7 | 0.064 | 35 | −0.38 |
| 1.1 | 0.074 | 46 | −0.12 |
| 1.3 | 0.078 | 65 | +0.38 |
| 1.5 | 0.082 | 75 | +0.68 |
| 1.9 | 0.089 | 85 | +1.04 |
| 2.3 | 0.095 | 95 | +1.65 |

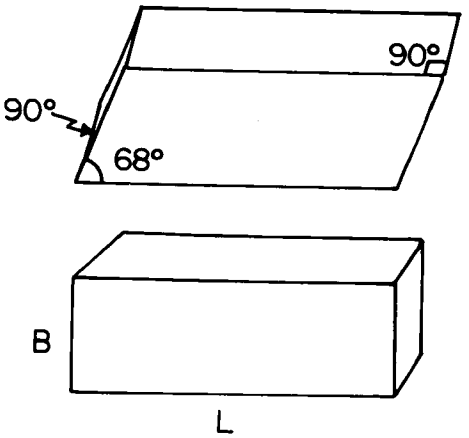


**Figure 2**—*Actual (top) and idealized (bottom) crystals of oxalic acid dihydrate.*

average (0.070 *versus* 0.0715 cm) and the mesh limits (0.048–0.095 cm). Furthermore, the average volume in Table II (0.73 × $10^{-3}$ ml) multiplied by the density of oxalic acid dihydrate (1.6 g/ml) gives a result fairly close to the correct weight per particle (1.2 *versus* 1.0 mg).

It is seen from Fig. 3 that the particles within the mesh fraction of a nonisothermally crystallized powder are fairly *normally* distributed[7]. Since the log-normally distributed powders are made by mixing mesh fractions in log-normal ratios, the powders can only be claimed to be approximately log normal, since the distribution within the fractions themselves is normal[7]. Brooke (25) discussed the ramifications of the use of mean mesh size diameters on the results of cube root dissolution.

One assumption made in deriving both Eqs. 4 and 5 is that the particles dissolving are isometric; *i.e.*, the surface area, $O$, can be related to the volume, $Q$, by:

$$O = \gamma(Q)^{2/3} \qquad \text{(Eq. 6)}$$

If, as seen in Fig. 2, the volume $Q = LB^2$ and the surface $O = 2B^2 + 4BL$, then $Q$ and $O$ cannot be placed in a relationship as dictated by Eq. 6 without involving $B$ and $L$. For an isometric shape, *e.g.*, a sphere, the relationship in Eq. 6 is obtained without involvement of dimensions [the factor $\gamma$ being $(36\pi)^{1/3}$ for a sphere].

It was found microscopically that $L = 2.7B$ on the average. If this is the case throughout the dissolution, then $Q = 2.7B^3$ and $O = 2B^2 + 10.8B^2 = 12.8B^2$. This would lead to $O/[Q^{2/3}] = 10.3$, independent of $B$ or $L$, so that the particles can be considered isometric only if the ratio stays constant at 2.7 during the dissolution.

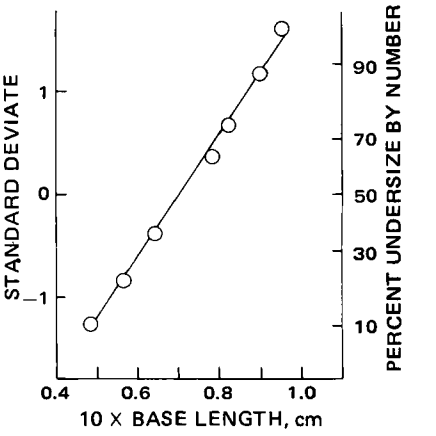


**Figure 3**—*Distribution of* B *values of oxalic acid dihydrate crystal of a −20/+30-mesh fraction.*

[7] This result is due to the fact that the −20/+30 cut is close to the "mean" of the nonisothermally recrystallized sample. Other cuts may be of a triangular distribution.

**Table III—Results from Three Different Runs under Identical Experimental Conditions (Mean = 1050 μm, σ = 0.21)**

| Seconds | $-\Delta\sqrt[3]{W}$, g$^{1/3}$, Run 1 | $-\Delta\sqrt[3]{W}$, g$^{1/3}$, Run 2 | $-\Delta\sqrt[3]{W}$, g$^{1/3}$, Run 3 | $-\Delta\sqrt[3]{W}$, g$^{1/3}$, Average | Letter Designation in Fig. 5 |
|---|---|---|---|---|---|
| 15 | 0.43 | 0.40 | 0.49 | 0.44 | A |
| 30 | 1.02 | 0.93 | 0.96 | 0.97 | B |
| 40 | 1.31 | 1.24 | 1.21 | 1.25 | C |
| 50 | 1.59 | 1.50 | 1.53 | 1.54 | D |
| 60 | 1.83 | 1.72 | 1.72 | 1.76 | E |
| 70 | 2.11 | 2.00 | 1.95 | 2.03 | F |
| 80 | 2.30 | 2.15 | 2.13 | 2.20 | G |
| 90 | 2.48 | 2.33 | 2.30 | 2.37 | I |
| 105 | 2.70 | 2.54 | 2.55 | 2.60 | H |
| 120 | 2.91 | 2.85 | 2.79 | 2.85 | J |

It was stated previously (15, 16) that the particles should dissolve isotropically (*i.e.*, the dissolution rate constants should be independent of the face of the crystal). This assumption is, however, not rigid, as will be shown. As noted in Fig. 2, there are four surfaces with an area of size $LB^2$. A decrease in $B$ is due to dissolution from the sides of area $LB$, so the dissolution rate constant for these faces is denoted $k_B$. Similarly, there are two sides with areas of size $B^2$ and a dissolution rate constant of $k_L$, so that dissolution from the crystal occurs with the rate:

$$-dm/dt = [4k_BLB + 2k_LB^2]C_s \qquad \text{(Eq. 7)}$$

If the length-to-breadth ratio is now denoted as $f = L/B$, then Eq. 7 may be written:

$$-dm/dt = B^2[4k_Bf + 2k_L]C_s \qquad \text{(Eq. 8)}$$

Since $Q = LB^2 = fB^3$, it follows that $-(dm/dt) = -\rho(dQ/dt) = -3\rho fB^2(dB/dt)$, so the equation becomes:

$$-dB/dt = [4k_Bf + k_L]/(3\rho f) \qquad \text{(Eq. 9)}$$

For Eqs. 4 and 5 to be structurally correct, $dB/dt$ must be constant, which it is if $f$ is time independent, *i.e.*, if the particle is isometric throughout the dissolution. It is granted that this isometry is related to it being isotropic, but it is fairly easy to check the constancy of $f$ by conducting a dissolution rate experiment on a single crystal under the microscope. The results of such experiments are shown in Fig. 4; the dimensions decrease linearly with time, implying that $[4k_Bf + 2k_L]/(3\rho f)$ is time independent. The original $f$ value is 0.12/0.045 = 2.7; after 100 sec (when 67% of the crystal is dissolved), the ratio is 0.09/0.03 = 3, *i.e.*, not much different.

The first dissolution rate experiment was carried out at one particular standard deviation and one particular mean. It was carried out three times to check reproducibility and to allow statistical evaluation of the critical time (Table III and Fig. 5). Visual examination of Fig. 5 supports the predicted biphasic nature of the cube root plots and of the existence of critical times. To show this result in a more quantitative manner, the three sets of experiments in

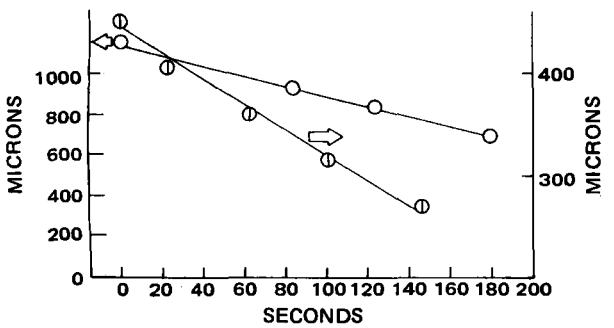


**Figure 4**—*Dissolution of single crystal of oxalic acid dihydrate at 25° in 0.2 ml of 0.1* N *HCl as determined microscopically. Left axis is length,* L, *of crystal; right axis is breadth,* B, *of crystal.*

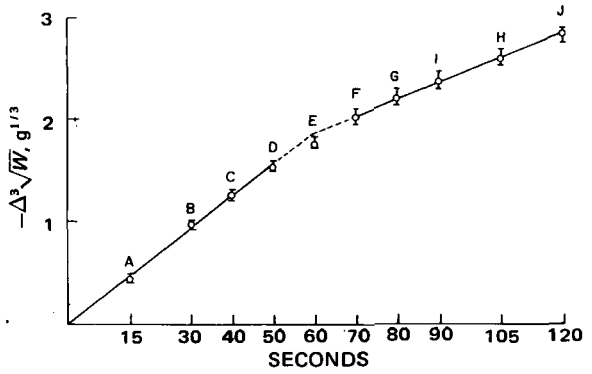


**Figure 5**—*Results from three different runs under identical experimental conditions; mean = 1050 μm and* SD = *0.21.*

Table III were subjected to statistical analysis. A linear regression analysis with nonzero intercept was carried out on the first four points (A, B, C, and D), and it was shown that the intercept was not significantly different from zero. The points were then fitted by least-squares fitting, and the following equation ensued:

$$-\Delta\sqrt[3]{W} = (0.0308 \pm 0.0014)t \qquad \text{(Eq. 10)}$$

The data points F, G, H, I, and J were then fitted by least-squares fitting, and the observed equation was:

$$-\Delta\sqrt[3]{W} = 0.0163t + 0.894 \qquad \text{(Eq. 11)}$$

By equating Eq. 11 with Eq. 10, one obtains: (*a*) the lower limit for $t_c$ = 56 sec, (*b*) the average value for $t_c$ = 62 sec, and (*c*) the upper limit for $t_c$ = 68 sec.

To show that the curve *is* biphasic, an alternative fit to the set of data was considered. This fit was a monophasic smooth curve, namely a power function of the type $y = ax^n$. The data were fitted to this equation by the method of least squares (Table IV), and the least-squares fit was found to be:

$$\tilde{y} = -\Delta\sqrt[3]{W} = 0.0455t^{0.882} \qquad \text{(Eq. 12)}$$

If this curve is a proper type with which to fit the data, then the deviations from the actual points ($y$ values) to those of Eq. 12 should alternate in sign in fairly random fashion as shown by Durbin and Watson (26). It can be seen from Table IV that this is not the case; six negative deviations occur followed by three positive. A similar argument holds for other smooth curves tested ($[1/y] = a[1/x] + b$ and $y = a[1 - \exp(bx)]$).

In general, in the following, $t_c$ values were obtained in this fashion; the cutoff points between the "first" and "last" points were always determined visually at first and then justified by inclusion of an extra point and demonstration of an increase in the residual sum of squares divided by $n - 2$ ($s_{yx}^2$). The $t_c$ values obtained in this fashion are ±10%.

Equation 5 may be written:

$$1 - \sqrt[3]{(W/W_0)} = \exp(c\sigma_D^2)\frac{2kC_s}{\rho M}t \qquad \text{(Eq. 13)}$$

This equation will be called a "reduced" form in the following discussion. Equation 4, of course, can be written in reduced form as

**Table IV—Points in Fig. 5 Plotted as a Power Function: $\tilde{y} = -\Delta\sqrt[3]{W} = 0.0455t^{0.882}$**

| Seconds | $\tilde{y}$ | $y$ | $\Delta = \tilde{y} - y$ |
|---|---|---|---|
| 15 | 0.496 | 0.44 | +0.056 |
| 30 | 0.914 | 0.97 | −0.056 |
| 40 | 1.178 | 1.25 | −0.072 |
| 50 | 1.434 | 1.54 | −0.106 |
| 60 | 1.684 | 1.76 | −0.076 |
| 70 | 1.929 | 2.03 | −0.101 |
| 80 | 2.170 | 2.20 | −0.029 |
| 90 | 2.408 | 2.37 | +0.038 |
| 105 | 2.759 | 2.60 | +0.159 |
| 120 | 3.103 | 2.85 | +0.253 |

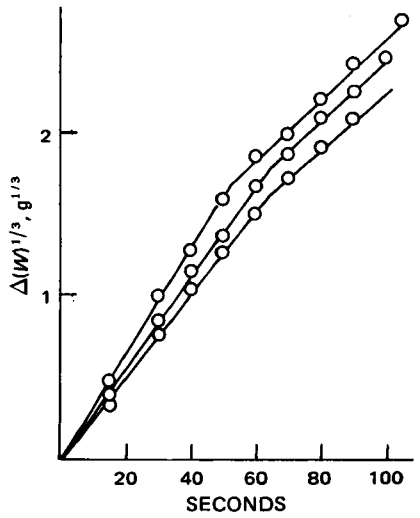


**Figure 6**—*Dissolution pattern of oxalic acid dihydrate of geometric mean 1500 μm and* SD *0.108 (top), 0.129 (middle), and 0.155 (bottom).*

well. According to this form, lines drawn according to the reduced equations should have slopes independent of the initial weight. To test this assumption, dissolution experiments were carried out with different amounts of oxalic acid dihydrate. The results are listed in Table V; the calculated rate constants are quite independent of the initial amount of solid.

Dissolution rate tests were performed at 25° on powders of identical mean diameter but with different standard deviations (Fig. 6). The slopes of the lines, after division by $\sqrt[3]{W_0}$ (=4.3), should, according to Eq. 13, follow the equation:

$$\ln [\text{slope}/\sqrt[3]{W_0}] = c\sigma_D^2 + \ln (2kC_s/[\rho M]) \quad \text{(Eq. 14)}$$

The plot of the data in Fig. 6 according to Eq. 14 are shown in Fig. 7; the linearity is obvious, and the least-squares fit line of Fig. 7 is:

$$\ln [\text{slope}/\sqrt[3]{W_0}] = -3.07\sigma_D^2 - 4.744 \quad \text{(Eq. 15)}$$

According to Brooke (16, 17), $c = -2.54$, so that both the linearity of Fig. 7 and the numerical value (2.54 being close to 3.07) support his equation. Knowledge of the values of $C_s$, $\rho$, and $M$ allows calculation of $k$ from the intercept of Fig. 7; *i.e.:*

$$\ln [2kC_s/(M\rho)] = -4.744 \quad \text{(Eq. 16)}$$

Inserting the values $\rho = 1.60$ g/ml, $C_s = 0.157$ g/ml, and $M = 0.15$ cm gives:

$$k = 6.7 \times 10^{-3} \text{ cm/sec} \quad \text{(Eq. 17)}$$

Equation 14 may be written:

$$\ln [\text{slope}/\sqrt[3]{W_0}] = \ln (1/M) + c\sigma_D^2 + \ln (2kC_s/\rho) \quad \text{(Eq. 18)}$$

To test this equation, dissolution rate studies were conducted at 25° with samples of oxalic acid dihydrate having the same standard deviation and different means (Fig. 8). This plot is a straight

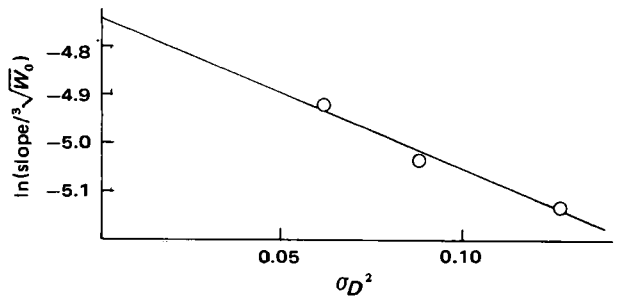


**Figure 7**—*Plot of weight-independent cube root slope* versus *variance of particle population.*

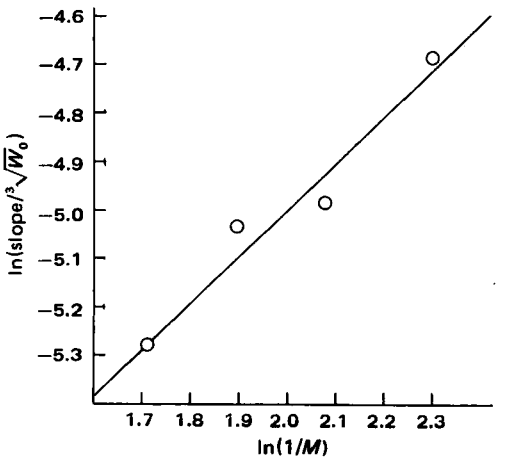


**Figure 8**—*Plot of weight-independent cube root slope* versus *reciprocal of geometric mean diameter.*

line as predicted by Eq. 18; it has a slope of 0.94 and should have a slope of unity.

Using the value of $c$ from Fig. 7 ($c = -3.07$) and the value of the intercept from Fig. 8 (−6.8752), one can now calculate $k$, since:

$$c\sigma_D^2 + \ln (2kC_s/\rho) = -6.8752 \quad \text{(Eq. 19)}$$

Inserting the values for $c$, $C_s$, $\rho$, and $\sigma_D = 0.3569$, one obtains:

$$k = 7.8 \times 10^{-3} \text{ cm/sec} \quad \text{(Eq. 20)}$$

Table V shows that the average weight-independent slopes of powders with a mean diameter of 1500 μm and a variance of $\sigma_D^2 = 0.0618$ have a value of $7.16 \times 10^{-3}$ sec$^{-1}$. Use of Eq. 14 and $c = -3.07$ gives a value of $k$ of:

$$k = 6.7 \times 10^{-3} \text{ cm/sec} \quad \text{(Eq. 21)}$$

Although they are not identical, the three $k$ values in Eqs. 17, 20, and 21 are of the same order of magnitude. This result supports the views stated in this report.

According to Eq. 5, the slope, $\alpha$, of a cube root plot is given by:

$$\alpha = \{\exp[c\sigma_D^2]\}\sqrt[3]{W_0}\,2kC_s/(\rho M) \quad \text{(Eq. 22)}$$

Inserting $c = -3.07$, $\sigma_D^2 = 0.0618$, $M = 0.15$ cm, $\rho = 1.60$ g/ml, and $\sqrt[3]{W_0} = 4.3$ g$^{1/3}$, one gets the simpler expression:

$$\alpha = 29.64kC_s \quad \text{(Eq. 23)}$$

The effect of temperature on dissolution is shown in Fig. 9 (and Fig. 4 for 25°). To examine the temperature dependence of $\alpha$, it is

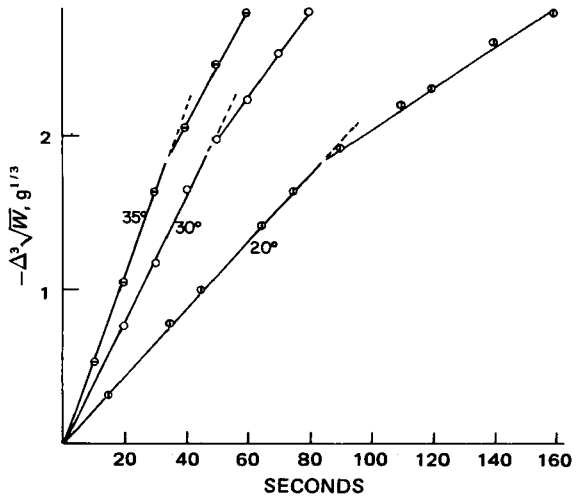


**Figure 9**—*Cube root plots as a function of temperature; mean = 1500 μm and* SD *= 0.108. The 25° data are shown in Fig. 4.*

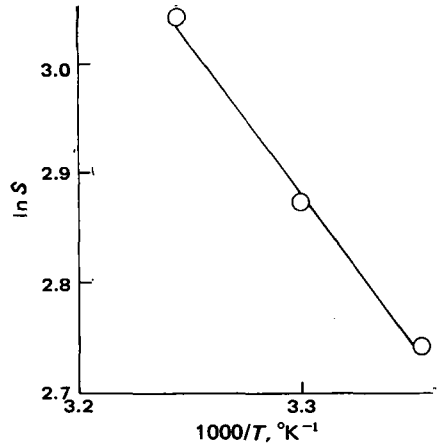


**Figure 10**—*Solubility–temperature plot of oxalic acid dihydrate.*

necessary to know the temperature dependence of $C_s$ and $k$; $C_s$ was determined experimentally at various temperatures (Fig. 10). The least-squares fit of the line is:

$$\ln C_s = -\frac{2751}{T} + 7.355 \qquad \text{(Eq. 24)}$$

where $C_s$ is expressed as grams per milliliter. If the viscosity of the dissolving medium (here assumed to be equal to the viscosity of water) is denoted $\eta$ and $r$ is the radius of the dissolved molecule, then the Stokes–Einstein equation requires that:

$$k = \frac{1.38 \times 10^{-16} T}{hr6\pi\eta} \qquad \text{(Eq. 25)}$$

From Eqs. 23 and 25, the following expression is obtained:

$$\alpha = [(29.64)(1.38 \times 10^{-16})/6\pi]\, C_s T/(hr\eta) = 2.17 \times 10^{-16} C_s T/(hr\eta) \qquad \text{(Eq. 26)}$$

It is noted that $(hr)$ is an unknown quantity. If it is assumed to be temperature independent over the temperature range studied, then:

$$\ln(\alpha/T) = -\ln(\eta) + \ln C_s + \ln[2.17 \times 10^{-16}/(hr)] = -\ln(\eta) + \ln C_s - \ln(hr) - 36.07 \qquad \text{(Eq. 27)}$$

The temperature dependence of the viscosity of water is:

$$\eta = 1.01 \times 10^{-5} \exp(2002/T) \qquad \text{(Eq. 28)}$$

or:

$$\ln(\eta) = 2002\,(1/T) - 11.434 \qquad \text{(Eq. 29)}$$

Inserting Eqs. 24 and 29 into Eq. 27 gives:

$$\ln(\alpha/T) = -\frac{4737}{T} - 17.29 - \ln(hr) \qquad \text{(Eq. 30)}$$

The data from Fig. 9 are plotted according to Eq. 30 in Fig. 11 and the linearity is obvious. The least-squares fit is:

$$\ln(\alpha/T) = -\frac{4760}{T} + 6.756 \qquad \text{(Eq. 31)}$$

That the slopes are identical is evident, although the proximity of the two values in Eqs. 30 and 31 is accidental. Experimental error is such that agreement to within 10% is considered adequate.

**Table V—Dissolution with Various Amounts of Initial Powder, $W_0$, of a Powder with Mean Diameter of 1500 μm and *SD* 0.108 in 0.1 *N* HCl at 25°**

| $W_0$, g | $W_0^{1/3}$, $g^{1/3}$ | Slope, $g^{1/3}$/sec | Slope/$(W_0^{1/3})$, $sec^{-1}$ |
|---|---|---|---|
| 80 | 4.3 | 0.0313 | $7.28\ 10^{-3}$ |
| 70 | 4.12 | 0.0281 | $6.84\ 10^{-3}$ |
| 60 | 3.91 | 0.0286 | $7.31\ 10^{-3}$ |
| 50 | 3.68 | 0.0263 | $7.15\ 10^{-3}$ |

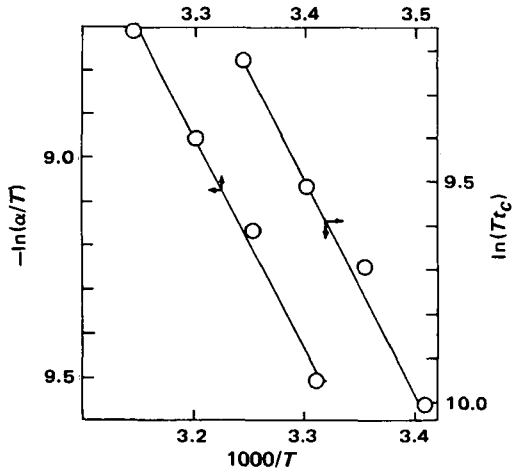


**Figure 11**—*Arrhenius plots of slope divided by absolute temperature (left) and critical time multiplied by absolute temperature (right).*

The intercept from Eq. 31 equals that from Eq. 30, so:

$$6.76 = 17.29 - \ln(hr) \qquad \text{(Eq. 32)}$$

*i.e.*, $\ln(hr) = -24.05$, so that:

$$hr = \exp(-24.05) = 4 \times 10^{-11} \qquad \text{(Eq. 33)}$$

Since $r$ is of the order of $10^{-8}$–$10^{-7}$ cm, $h$ would be of the order of 40–4 μm, which is of the expected order of magnitude (3).

Carstensen and Musa (15) showed that the critical time is given in terms of the smallest diameter, $a_0$, by:

$$t_c = a_0\rho/(2kC_s) \qquad \text{(Eq. 34)}$$

so that Arrhenius plots of $t_cT$ should have the same numerical slope with opposite sign as Arrhenius plots of $\alpha/T$. This is the case, as demonstrated in Fig. 11. The definition of $a_0$ for an actual crystal is vague, and the fact that allows comparison is that all of the powders in Fig. 11 have the same particle distribution and, hence, the same $a_0$ by whatever definition.

## SUMMARY

1. The experimental data presented here demonstrate that initially a powder with log-normal distributed dimensions will dissolve under sink conditions *via* a cube root law as predicted previously (15–17). The plots eventually are biphasic.

2. The dependence of the slopes of the cube root plots on the mean diameter and on weight is as described previously (15).

3. The dependence of the slopes of the cube root plots on the standard deviation of the powder distribution is as described previously (17).

4. The temperature dependence of the slopes of the cube root and of the critical times was derived theoretically and substantiated by experiment.

## REFERENCES

(1) P. Pothisiri and J. T. Carstensen, *J. Pharm. Sci.*, **62**, 1468(1973).

(2) A. Hussain, *ibid.*, **61**, 811(1972).

(3) D. Wurster and P. Taylor, *ibid.*, **54**, 169(1965).

(4) J. T. Carstensen, "Pharmaceutics of Solids," Badger-Freunc, Fon du Lac, Wis., 1974, pp. 62–67, 87, 133.

(5) A. Hixson and J. Crowell, *Ind. Eng. Chem.*, **23**, 923(1931).

(6) A. Noyes and W. Whitney, *Z. Phys. Chem.*, **23**, 689(1897).

(7) G. Steiner, M. Patel, and J. T. Carstensen, *J. Pharm. Sci.*, **63**, 1395(1974).

(8) J. T. Carstensen and M. Patel, *ibid.*, **63**, 1494(1974).

(9) G. Herdan and M. L. Smith, "Small Particle Statistics," Elsevier, New York, N.Y., 1953.

(10) G. L. Beyer, in "Technique of Organic Chemistry," vol. I,

part I, A. Weissberger, Ed., Interscience, New York, N.Y., 1949, p. 197.
(11) T. Hatch and S. P. Choate, *J. Franklin Inst.*, **207**, 369(1929).
(12) E. Parrot, in "The Theory and Practice of Industrial Pharmacy," 1st ed., L. Lachman, H. A. Lieberman, and J. L. Kanig, Eds., Lea & Febiger, Philadelphia, Pa., 1970, p. 115.
(13) W. I. Higuchi and E. N. Hiestand, *J. Pharm. Sci.*, **52**, 67(1963).
(14) W. I. Higuchi, E. L. Rowe, and E. N. Hiestand, *ibid.*, **52**, 162(1963).
(15) J. T. Carstensen and N. M. Musa, *ibid.*, **61**, 223(1972).
(16) D. Brooke, *ibid.*, **62**, 795(1973).
(17) *Ibid.*, **63**, 344(1974).
(18) J. H. Gaddum, *Nature*, **156**, 463, 747(1945).
(19) D. J. Finney, *J.R.S.S.*, **7**, Suppl. No. 2(1941).
(20) L. Z. Benet, in "Dissolution Technology," L. Leeson and J. T. Carstensen, Eds., American Pharmaceutical Association, Academy of Pharmaceutical Sciences, Washington, D.C., 1974, p. 30.
(21) L. F. Prescott, R. F. Steel, and W. R. Ferrier, *Clin. Pharmacol. Ther.*, **11**, 496(1970).
(22) J. B. Bookey and N. C. Tombs, *J. Iron Steel Inst.*, **172**, 86(1952).
(23) G. P. Baxter and J. E. Lansing, *J. Amer. Chem. Soc.*, **42**, 419(1920).
(24) E. Csontas, *Agrokem. Talajtan*, **5**, 425(1956).
(25) D. Brooke, *J. Pharm. Sci.*, **64**, 1409(1975).
(26) J. Durbin and G. Watson, *Biometrika, Part II*, **58**, 1(1971).

**ACKNOWLEDGMENTS AND ADDRESSES**

Received October 3, 1974, from the *School of Pharmacy, University of Wisconsin, Madison, WI 53706*
Accepted for publication February 13, 1975.
The authors are indebted to Mr. R. Sowinski and Mr. T. Lai.
[x] To whom inquiries should be directed.

# Controlled Drug Release from Polymeric Delivery Devices III: *In Vitro–In Vivo* Correlation for Intravaginal Release of Ethynodiol Diacetate from Silicone Devices in Rabbits

**YIE W. CHIEN [*x], STANLEY E. MARES [‡], JOHN BERG [‡], SUSAN HUBER [‡], HOWARD J. LAMBERT [*], and KENNETH F. KING [§]**

**Abstract** □ Forty female rabbits were implanted with silicone vaginal devices containing ethynodiol diacetate for up to 8 weeks. As predicted from *in vitro* studies, a $Q - t^{1/2}$ (matrix-controlled) release profile was observed *in vivo*. The *in vivo* drug release profile was compared with *in vitro* data measured at three hydrodynamic conditions, and the diffusional resistance across the vaginal wall was estimated. Drug released from silicone devices yielded a prolonged plasma level when compared with data following intravaginal or intravenous administration of a solution dose. The rate constant for elimination was unchanged. The plasma concentration of the drug was related to the intravaginal drug release profile both theoretically and experimentally and was above the concentration required to inhibit fertilization.

**Keyphrases** □ Drug delivery systems—controlled release, polymeric devices, ethynodiol diacetate in silicone matrix, *in vitro–in vivo* correlation of intravaginal release, rabbits □ Ethynodiol diacetate—intravaginal release from silicone matrix, *in vitro–in vivo* correlation, rabbits □ Silicone matrix—ethynodiol diacetate delivery system, *in vitro–in vivo* correlation for intravaginal release, rabbits □ Vaginal devices—controlled release of ethynodiol diacetate from silicone matrix, *in vitro–in vivo* correlation, rabbits

An *in vitro* drug release system, which allows a direct and rapid characterization of a drug release profile and mechanism, was recently reported from this laboratory (1). Two types of drug release mechanisms, matrix controlled and partition controlled, were observed when the drug release profiles of ethynodiol diacetate from silicone devices were followed daily in this system (2).

To develop a device with a desirable, long-acting, drug release profile, it is necessary to examine intravaginal drug release mechanisms in animals to establish an *in vitro–in vivo* correlation. This paper reports results of drug release studies with silicone devices containing ethynodiol diacetate placed in the vaginal tracts of 40 rabbits for up to 8 weeks.

## EXPERIMENTAL

***In Vitro* Release Studies**—The apparatus for *in vitro* drug release studies and the assay of drug samples were essentially the same as those reported previously (1). The ring-shaped silicone device, containing 112.6 mg/cm$^3$ of ethynodiol diacetate[1], was mounted in the arms of a Plexiglas holder and then rotated at 81 or 30 rpm or held stationary (to simulate more closely the status of implants in the vaginal lumen) in 150 ml of a 75% polyethylene glycol 400 solution as the elution medium at 37°. The solution was mixed well prior to sampling, and the drug concentration in the medium was assayed daily (1, 2). The reproducibility of the *in vitro* $Q/t^{1/2}$ profiles measured at various dates within 1 year was excellent (Table I).

***In Vivo* Release Studies**—The same silicone devices as those used in the *in vitro* drug release studies were cut into sections of 1 cm in length. One segment was inserted into the anterior vagina of each of 40 young adult New Zealand white female rabbits *via* a midventral laparoelytrotomy. It was anchored with a single polyethylene suture knotted on one side of the implant (through the implant perpendicular to the long axis) and then drawn through the vaginal wall and knotted to a 1-cm section of medical-grade tubing[2].

[1] SC-11800.
[2] Silastic, Dow Corning Corp., Midland, Mich.